Strain Induced Band Dispersion Engineering in Si Nanosheets

ARTICLE *in* THE JOURNAL OF PHYSICAL CHEMISTRY C · NOVEMBER 2011

Impact Factor: 4.77 · DOI: 10.1021/jp206911b

3 AUTHORS:

Chao Zhang
Yantai University
39 PUBLICATIONS **182** CITATIONS
SEE PROFILE

Abir De Sarkar
Institute of Nano Science and Technology
47 PUBLICATIONS **337** CITATIONS
SEE PROFILE

Rui Qin Zhang
City University of Hong Kong
326 PUBLICATIONS **5,680** CITATIONS
SEE PROFILE

THE JOURNAL OF PHYSICAL CHEMISTRY C

ARTICLE

pubs.acs.org/JPCC

Strain Induced Band Dispersion Engineering in Si Nanosheets

Chao Zhang,† Abir De Sarkar, and Rui-Qin Zhang*

Department of Physics and Materials Science, City University of Hong Kong, Hong Kong SAR, China

ABSTRACT: The electronic properties of strained hydrogen-passivated Si nanosheets are investigated using the first-principles density functional theory. Asymmetrical strain has been found to cause a direct-to-indirect transition in the (100) Si nanosheet, while symmetrical strain retains its direct band gap characteristic. Under asymmetrical strain along the ⟨100⟩ direction, the direct band gap of the (110) Si nanosheet exhibits unique characteristics, with the direct band gap varying linearly with strain. Similar band gap variation behaviors are observed for the (110) Si nanosheet subject to symmetrical and asymmetrical strains along the ⟨110⟩ direction. The various strain dependences are attributed to the changes in its charge density. Our results can be used to guide the strain engineering of the electronic properties of low-dimensional silicon materials.

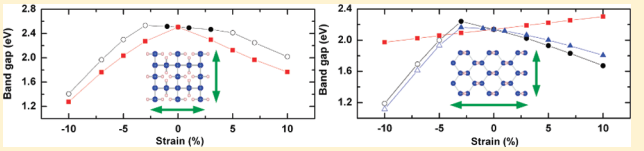

1. INTRODUCTION

Silicon, the second most abundant element in the earth's crust, has been exploited in numerous applications for its amazingly useful properties. For instance, silicon is the cornerstone of the semiconductor industry. Moreover, it also offers itself as a model system for probing into the structure−property relationship. The continued trend for miniaturization of electronic devices induces the genesis of novel properties, which in turn incorporate themselves into the devices. As the silicon-based materials shrink down to the nanoscale, manifold interesting changes show up: the indirect band gap gradually transforms itself into a direct band gap semiconductor, the energy band gap widens, and the surface to volume ratio increases. The sum-total of the unprecedented bonuses accruing from the downsizing of Si-based materials is commonly known as quantum size effect or quantum confinement effect. The significant increase in the surface area with the down-scaling of materials provides plenty of room for functionalization of the surface. Consequently, in low dimensional materials, the surface comes to the center stage and plays the key role, while the bulk takes a back seat. In the nano realm, silicon appears in a variety of structures, such as zero-dimensional (0D) quantum dots,[1] one-dimensional (1D) nanowires,[2,3] and two-dimensional (2D) nanosheets.[4,5] These low-dimensional Si nanotructures exhibit diverse electronic properties, due to quantum confinement in different dimensions, and have drawn the attention of the scientific community for extensive investigations. The past decade has witnessed a surge of research interests in the structures and properties of 2D materials in the nano realm, which has been partially boosted by the development of single-layer graphite (graphene), especially the preparation of free-standing graphene using mechanical exfoliation in 2004.[6] Benefiting from the advancement in nanotechnology, the layered nanostructures of silicon with atomic thickness, often called nanosheet, have been successfully synthesized.[4,5,7,8] Very recently, the silicon nanoribbons grown epitaxially on silver (110) and (100) surfaces paved the way for the synthesis of graphene-like silicon nanosheets.[9−11] Nanosheets bridge the gap between 1D nanomaterials and three-dimensional (3D) macroscale bulk materials and will thereby advance our understanding of the quantum confinement effect across the boundaries of all dimensions in materials science. Even in the same dimension, the subtle shape difference can lead to totally different properties. For example, in its 1D structure, the electronic band structure of SiNWs depends strongly on the wire diameter and growth direction.[12] Therefore, it turns out that the advances in nanoelectronics will be primarily driven by the taming of the structures of Si nanomaterials for the purpose of tailoring their electronic properties.

Besides structural manipulation mentioned in the foregoing paragraph, surface functionalization (or surface chemistry) is also frequently employed to alter the electronic properties of Si nanomaterials, as surface gains prominence relative to the bulk in low dimensional systems. H-terminated Si quantum dots, which usually emit energies above 3.0 eV in the blue region is found to shift to the yellow-red region of the spectrum in its oxidized state, emitting energies near 2.0 eV.[1] Surface passivation of SiNWs by specific adsorbates (or simply surface chemistry/functionalization of SiNWs in another parlance) have found useful applications in the modulation of its electrical properties by inducing a charge separation between the SiNW and the adsorbate layer.[13] This charge separation (i.e., creation of quasiparticle excitons or electron−hole pairs) across the interface is also sometimes referred to as doping as it enhances the conductivity of SiNWs substantially.[14,15] Interestingly, doping here is introduced by surface chemistry as the surface is the main player in low-dimensional systems, in contrast to the bulk in 3D macroscopic materials. The phenyl-modified[8] and H-terminated[16] silicon nanosheets exhibit incredible opto-electronic properties, demonstrating their potential for applications in luminescence and solar cells.[5] In addition, the application of external strain has lately

Received: July 20, 2011
Revised: October 26, 2011
Published: October 26, 2011

dx.doi.org/10.1021/jp206911b | J. Phys. Chem. C 2011, 115, 23682–23687

been found to be one of the most promising strategies for developing high-performance nanoscale devices. Recently, strain has been used to enhance mobility in planar Si metal-oxide-semiconductor field-effect transistors.[17] There have been a few attempts to tailor the optical properties of SiNWs by strain engineering.[18,19] Strain arises naturally during the synthesis of NWs: compressive radial strain and tensile axial strain in the SiNWs is found to occur due to the facile formation of an amorphous SiO_2 layer (1−2 nm thick) on its surface upon its exposure to air.[20] Strain also exists in core−shell NWs due to a lattice mismatch between the different elements used. For instance, a low percentage of strain was found in Si/Ge core−shell NWs.[21−23] As compared to 1D SiNWs, the investigations of strain effect on 2D Si nanosheets are relatively few, partly due to the difficulties experienced in the synthesis of free-standing Si nanosheets.[5,8,10] Herein, we explore the possibility of using strain to manipulate the electronic band structures of Si nanosheets, while focusing on its most widely investigated (100) and (110) facets. Our results indicate that strain can tune not only the magnitude of the band gap but also the band dispersion (i.e., direct or indirect band gap), which has crucial implications for the applications of Si nanosheets in opto-electronics, luminescence, and solar cells.

2. COMPUTATIONAL DETAILS

Our first-principles calculations are based on the density functional theory (DFT) within a generalized gradient approximation (GGA).[24] We have used the projector-augmented wave method[25] and a plane-wave basis set, as implemented in the VASP package.[26,27] The cutoff energy has been set to 350 eV, and a 10 × 10 × 2 Monkhorst-Pack[28] k-point grid has been used to ensure the k-mesh spacing to be smaller than $2\pi \times 0.03$ Å^{-1}. We constructed the Si nanosheets in the bulk silicon crystal along the (100) and (110) directions. The Si nanosheets with the thinnest Si layers in the periodic supercells were decoupled by a vacuum thickness larger than 15 Å. The (100) Si nanosheet contains three Si layers with a thickness of 2.58 Å, while the (110) Si nanosheet comprises two Si layers with thickness of 1.88 Å. The structures were relaxed using a conjugate gradient method with the convergence criteria for energy and forces set to 1×10^{-5} eV/supercell and 0.01 eV/Å, respectively.

The application of tensile and compressive axial strains were simulated by scaling the lattice constant along the two mutually perpendicular directions of the nanosheet, and this method has been successfully used to study the strain effects on nanowires.[29−34] The positive values of strain refer to expansion, while negative values correspond to contraction. After changing the box size, the coordinates of all atoms were allowed to relax to the equilibrium structure. The extent of the applied strain considered in our computational investigations is ±10%. A considerably large strain studied in theoretical calculations[35] may not be easily realizable in experiments. However, the trend predicted by first-principles calculations will facilitate a clearer understanding of the underlying physics, which in turn will provide useful pointers to experimental efforts.

3. RESULTS AND DISCUSSION

We have first characterized the geometries of Si nanosheets free from any strain. The dangling bonds on the surfaces of silicon nanosheets of the (100) and (110) facets, constructed in our model, were passivated by hydrogen. The (100) and (110) Si

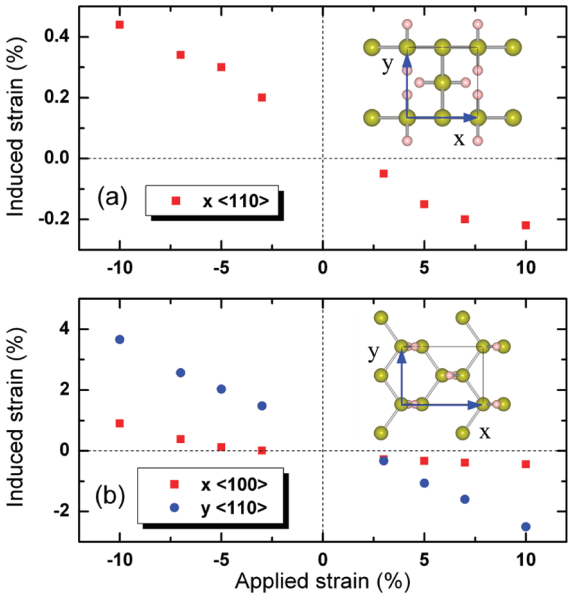

Figure 1. Induced strain as a function of applied strain for the (a) (100) Si nanosheet and the (b) (110) Si nanosheet. The insets are the ball and stick models representing the atomic arrangement where the big and small spheres denote silicon atoms and hydrogen atoms, respectively.

nanosheets have D_{2d} and D_{2h} symmetries, respectively, and therefore, the size is initially set to $a_x = a_y = 3.84$ Å for the (100) Si nanosheet, and $a_x = (2)^{1/2}a_y$, $a_y = 5.43$ Å, for the (110) Si nanosheet. Then, we have performed a series of calculations of the total energy with different lattice constants for a given nanosheet, and the in-plane lattice constants were obtained at the equilibrium, ground state of the system, corresponding to the minimum in its total energy. This method has already been validated for the study of the strain effects.[35] The calculated in-plane lattice constants of both Si nanosheets are found to be greater than the initial input. For example, $a_x = a_y = 4.07$ Å were obtained for the (100) Si nanosheet. This indicates the expansion of the nanosheet perpendicular to the xy plane containing the nanosheet (i.e., the z direction), and this phenomenon is also observed in nanowires (NWs).[23,33,34]

The (100) Si nanosheet is stretchable along two equivalent ⟨110⟩ directions. Consequently, there exist two modes for applying axial strain on it: (i) symmetrical strain along the x and y directions and (ii) asymmetrical strain along the x or y direction. When an asymmetrical strain is applied to the Si nanosheet along x, the nanosheet will contract along the y direction. Along the x direction, the ratio of the changed lattice constant to the strain-free, optimized lattice constant refers to the applied strain. For a fixed lattice constant along the x direction, a series of total energy calculations have been performed using different lattice constants along the y direction. Along the y direction, the lattice constant corresponding to the energy minimum refers to the changed lattice constant, and its ratio to the strain-free lattice constant is termed as the induced strain. Figure 1a shows the induced strain as a function of strain applied to the (100) Si nanosheet. When subjected to the same degree of applied strain, the nanosheet is found to be more sensitive to compressive strain than to tensile strain. For example, a +5% (−5%) applied strain induces −0.15% (0.3%) strain. This implies that the (100) Si nanosheet is relatively readily compressible along the ⟨110⟩ direction, as compared to the other direction.

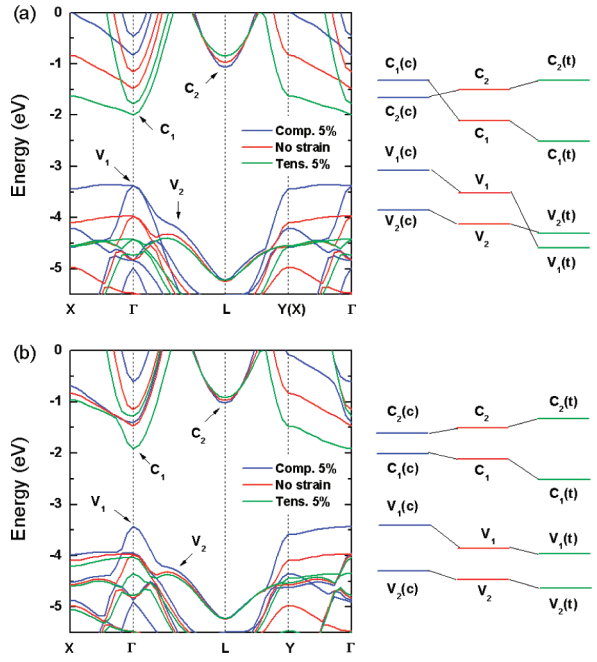

Figure 2. Electronic band structure (left panel) and schematic description of the evolution of energy states (right panel) of the (100) Si nanosheet under (a) symmetrical strain and (b) asymmetrical strain. The c and t in parentheses denote compressive and tensile strains, respectively.

The modes of applying strain to the (110) Si nanosheet are somewhat different from that of the (100) Si nanosheet, due to the two nonequivalent directions. The structure sensitivity of the (110) Si nanosheet to the strain application along the ⟨100⟩ and ⟨110⟩ directions is shown in Figure 1b. The applied strain along the ⟨110⟩ (y) direction induces a much larger strain. In particular, 10% of the compressive strain along the ⟨110⟩ direction induces 3.7% expansion along the ⟨100⟩ direction, the largest induced strain. Similar to the (100) Si nanosheet, applied compressive strain induces a larger strain. For example, a +5% asymmetrical strain applied along the y direction induces −1.1% strain, but a +5% asymmetrical strain applied along the x direction can produce only −0.33% induced strain. It may be inferred from these results that the (110) Si nanosheet is more sensitive to the application of compressive stress along the ⟨110⟩ direction.

Figure 2 shows both the symmetric and asymmetric strain dependences of the electronic band structure of the (100) Si nanosheet. The shape and high symmetry points of the Brillouin zone can be found in our previous paper.[16] As the light emission or absorption of silicon-based nanostructures depends strongly on the band gap, we have labeled the energy states in Figure 2, which crucially determine the band gap, such as C_1 for the energy state at the conduction band edge. The energy states at point Y show a behavior similar to that at point Γ under strain, but they do not play a dominant role in the band gap transition and are therefore omitted in the following discussion. When no strain is applied to the (100) Si nanosheet, the energy differences between V_1 and V_2 ($\Delta V = V_1 - V_2$) and the same between C_1 and C_2 ($\Delta C = C_2 - C_1$) are 0.36 and 0.50 eV, respectively. It is noted here that a positive value of ΔV (ΔC) implies that the energy V_1 (C_2) is higher than V_2 (C_1). If both ΔV and ΔC are positive, a direct band gap is favored for the (100) Si nanosheet. Notice that a direct band gap enhances its optical efficiency (i.e., light absorption/emission), and consequently, it has potential for opto-electronic applications. When symmetrical compressive strain is applied to the (100) Si nanosheet, the C_1, V_1, and V_2 states rise in energy, while the C_2 state drops energetically. When the compressive strain is large enough to induce a negative ΔC value, the Si nanosheet undergoes a direct-to-indirect transition. Contrary to the compressive strain effect, the C_1, V_1, and V_2 states are downshifted in energy when symmetrical tensile strain is applied to the Si (100) nanosheet. Interestingly, the magnitude of the downward shift of V_1 is much larger than that of V_2, yielding a negative ΔV. On the basis of these, it can be concluded that both symmetrical compressive and tensile strains can easily alter the electronic band dispersion of the (100) Si nanosheet from a direct band gap to an indirect band gap.

The effect of asymmetrical strain on the band structure of the (100) Si nanosheet is somewhat different from that of the symmetrical strain. Similar to the case of symmetrical compressive strain, the C_1, V_1, and V_2 states are shifted up in energy, while the C_2 state is downshifted. However, the extent of the upward shift of the C_1 state is small, leading to a positive ΔC, such as 0.38 eV at 5% compressive strain. Thus, the (100) Si nanosheet preserves the direct band gap up to 10% compressive strain. When asymmetrical tensile strain is applied to the Si nanosheet along the ⟨110⟩ direction, all of these involved energy states show totally different behaviors, leading to positive values for both ΔC and ΔV. Thus, within our studied range of applied strain, we observe that the application of asymmetrical compressive strain retains the direct band gap dispersion of the (100) Si nanosheet, while the tensile strain enhances the direct band gap.

The different strain dependences of the V_1, V_2, C_1, and C_2 states can be understood from decomposed charge density, as shown in Figure 3. The decomposed charge density of the C_1 state shows a zigzag spatial distribution, surrounding closely the Si atoms from the two mutually perpendicular directions. Interestingly, the zigzag-shaped decomposed charge density occurs parallel to the Si bonds. The decomposed charge density of the V_1 state encircles the Si−Si bonds and Si−H bonds. The decomposed charge densities of the C_1 and V_1 states reflect the bonding character of the (100) Si nanosheet and are, therefore, very sensitive to structural changes. In response to the variation of the structures of the Si nanosheets with the external strain, the energy of the C_1 and V_1 states change rapidly. Moreover, both the decomposed charge densities of the C_1 and V_1 states distribute along two directions. The symmetrical strain can induce a considerable change. The decomposed charge density of the C_2 state distributes in the interatomic space between the Si atoms, while the decomposed charge density of V_2 distributes mainly in the xy plane of the nanosheet and normal to it (i.e., the z direction). They do not relate closely to the Si−Si bonds, and consequently, the structural change of the (100) Si nanosheet marginally influences the shape of the decomposed charge density corresponding to C_2 and V_2.

When the (110) Si nanosheet is free from strain, both the valence band (V_1) maximum and conduction band (C_1) minimum located at point Γ, show a direct band gap. Under strain, a state in the conduction band, labeled as C_2, participates in the direct-to-indirect band gap transition. The schematic strain dependences of these three energy states and the electronic band structure of the (110) Si nanosheet are shown in Figure 4. The behaviors of V_1 under symmetrical and asymmetrical strains are identical, as shown in the right panel of Figure 4. The energy of the V_1 state increases when subjected to compressive strain,

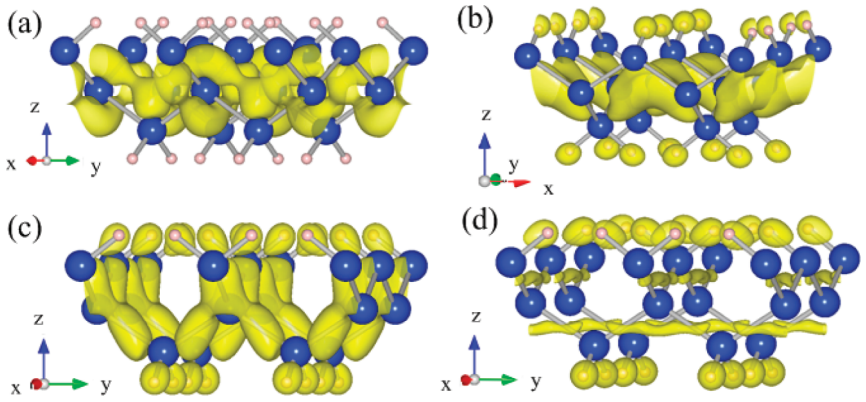

Figure 3. Isosurfaces of the electronic charge density corresponding to (a) C_1, (b) C_2, (c) V_1, and (d) V_2 in the (100) Si nanosheet. The isosurfaces in the figure show 35% of the maximum electronic charge density.

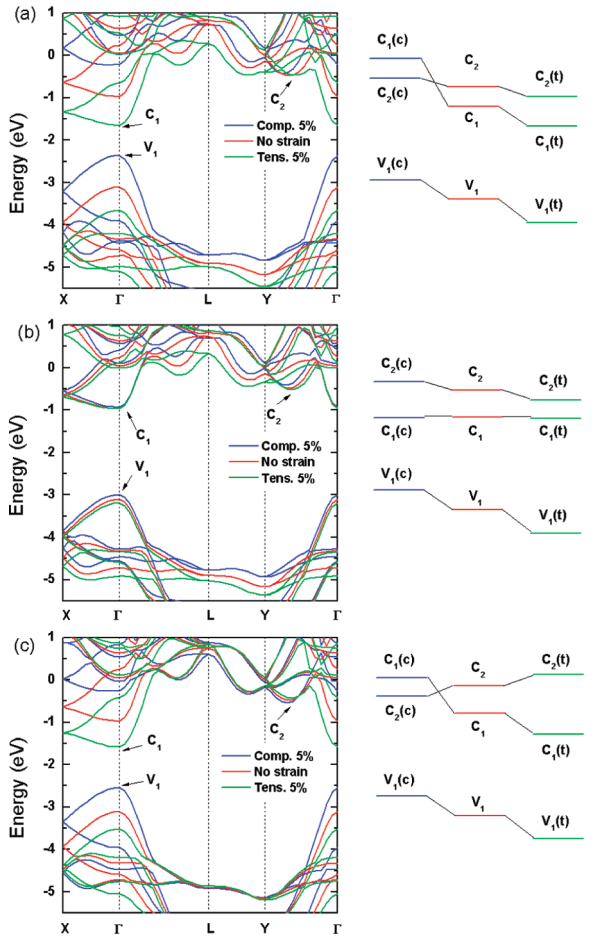

Figure 4. Electronic band structure (left panel) and schematic representation of the evolution of energy states (right panel) of the (110) Si nanosheet under (a) symmetrical strain and (b) asymmetrical strain along the x direction and (c) asymmetrical strain along the y direction. The c and t in parentheses denote compressive and tensile strains, respectively.

while it decreases under tensile strain, similar to the V_1 behavior in the (100) Si nanosheet. The C_2 energy state shows weak strain dependence, regardless of whether it is tensile or compressive strain. Thus, the other conduction band energy state, C_1 located at the Γ point, dominates the band gap characteristic. When symmetrical compressive strain is applied to the (110) Si nanosheet, the energy of C_1 rises. The value of ΔC becomes negative under sufficient compressive strain. As a result, the (110) Si nanosheet experiences a direct-to-indirect band gap transition. Contrary to the effect of compressive strain, the energy of the C_1 state decreases remarkably under symmetrical tensile strain, enlarging the direct band gap and its characteristics.

Interestingly, the energy of the C_1 state scarcely changes under asymmetrical strain along the x direction. The (110) Si nanosheet not only preserves the direct band gap characteristic but also shows amazing properties under asymmetrical strain. The detailed band gap evolution under asymmetrical strain is discussed hereafter. Under asymmetrical strain along the y direction, the electronic band structure of the (110) Si nanosheet is similar to that under symmetrical strain. The compressive strain induces a negative ΔC, and the tensile strain contributes positively to ΔC, enhancing the direct band gap.

The different strain dependences of C_1, C_2, and V_1, particularly the invariance of C_1 under asymmetrical strain along the x direction, can also be explained through decomposed charge density analysis. The semilunar shaped decomposed charge density corresponding to the C_1 energy state encloses each Si atom from one direction. The decomposed charge density of the C_1 distributes along the x direction, and a large part of it approaches the center of the distorted Si hexagon when viewed from the z direction, as shown in Figure 5a. By applying asymmetrical strain along the x direction, the shape of the decomposed charge density at C_1 does not change significantly. However, the asymmetrical strain along the y direction will affect the distribution of the decomposed charge density at C_1 qualitatively. Therefore, the energy of the C_1 state barely changes under asymmetrical strain along x, as denoted in Figure 4b. The decomposed charge density of V_1 encloses the Si−Si bond in the xy plane. A careful inspection of the shape of the decomposed charge density corresponding to V_1 reveals that its distribution projected along the x direction is larger than that projected along y, enhancing the sensitivity of the energy of V_1 to asymmetrical strain along y. With the same magnitude of strain, the increment of V_1 under asymmetrical strain along y is larger than that under asymmetrical strain along x, as seen in Figure 4b,c. Similar to the distribution of C_2 in the (100) Si nanosheet, the decomposed charge density of C_2 in the (110) Si nanosheet distributes itself in the interatomic space of the Si atoms and contributes weakly to

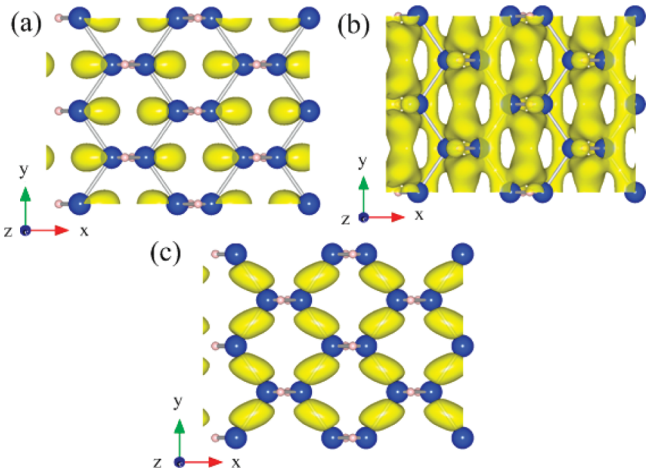

Figure 5. Isosurfaces of the electronic charge density at (a) C_1, (b) C_2, and (c) V_1 of the (110) Si nanosheet. The isosurfaces are 35% of the maximum density.

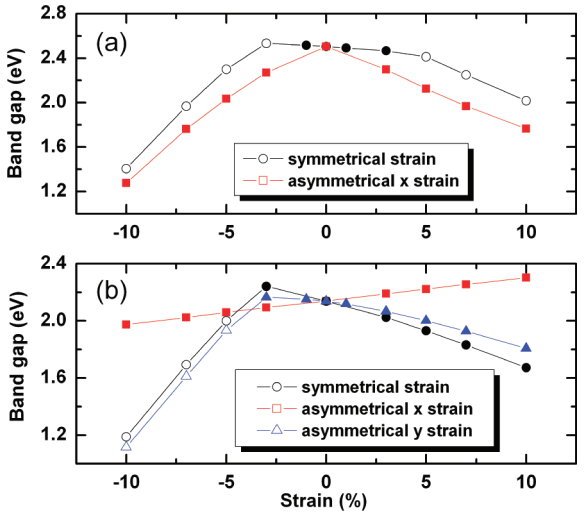

Figure 6. Band gap versus strain for (a) the (100) Si nanosheet and (b) the (110) Si nanosheet. Filled and unfilled symbols denote the direct and indirect band gaps, respectively.

Si−Si bonds. Thus, the energy of the C_2 state shows weak strain dependence. The variation of the band gap of the Si nanosheet with strain is shown in Figure 6. While DFT with a GGA functional is known to underestimate the band gap, more accurate quantum Monte Carlo calculations[36] and a GW approximation[37,38] have shown that DFT reproduces the general trends of the band gap variation. When free from strain, the (100) Si nanosheet tends to have a larger indirect band gap than that of the (110) Si nanosheet due to the larger quantum confinement. This trend holds good for symmetrically strained nanosheets. Therefore, unstrained (100) Si nanosheets have a stronger potential for solar cell applications than the (110) nanosheets because of the larger indirect band gap of the former.

Figure 6 shows clearly the strain tunability of the band gap of Si nanosheets. To obtain a smaller band gap, a larger strain (at least 5%) needs to be applied to the (100) Si nanosheet, as shown in Figure 6a. By carefully controlling the magnitude of the applied symmetrical compressive strain to the (100) Si nanosheet, a blue-shift followed by a red-shift of the spectrum can be induced in photoluminescence measurements. This owes its origin to the rise in energy of the C_1 state. To have a direct band gap in optical and luminescence applications, asymmetrical strain along the x direction, as shown in Figure 6a by filled squares, will have to be applied.

The variation of the band gap of the (110) Si nanosheet with strain is shown in Figure 6b. Interestingly, the magnitude of the direct band gap of the (110) Si nanosheets increase monotonically and linearly with asymmetrical strain along the x direction. On the basis of this behavior, one can get a larger band gap by applying tensile strain and a smaller gap by compressive strain. The unique band gap dependence accrues mainly from the C_1 energy state, whose energy remains almost nearly constant under asymmetrical strain along x. The smaller band gaps of direct type can also be obtained by applying symmetrical tensile strain and asymmetrical y tensile strain. Similar to the (100) Si nanosheet, a blue-shift followed by a red-shift will be observed in the spectrum, when symmetrical strain and asymmetrical compressive strain is consecutively applied along the y direction to the (110) Si nanosheet. This underscores the importance of strain engineering in Si nanosheets for applications in opto-electronics and luminescence. Furthermore, strain engineering of Si nanosheets can be utilized more conveniently and flexibly in its solar cell applications. The external strain can be realized experimentally by controllable deposition or epitaxial growth methods. For instance, Kim et al.[5] have observed strain in their free-standing Si nanosheets and strain-induced variation in optical properties.

In our previous work of ⟨112⟩ SiNWs,[29] we have found the axial compression or expansion to be effectual in altering the electronic bands near the Fermi energy level and eventually in inducing an indirect-to-direct band gap transition under a certain degree of strain, exhibiting the potential of SiNWs for applications in opto-electronics and luminescence. In comparison to SiNWs, the 2D Si nanosheets offer more accessible ways for applying strain to it. By carefully controlling the magnitude and direction of strain application, one can obtain different band dispersions (e.g., direct or indirect band gap) and band gaps of different magnitudes. Therefore, strain application can be an effective way for engineering the electronic band structure of silicon nanostructures.

4. CONCLUSIONS

In summary, strain induced tunability of the electronic band structure in Si nanosheets has been comprehensively addressed using the first-principles density functional theory in our work, and a microscopically clear understanding has emerged from the systematic investigations pursued. In conclusion, both (100) and (110) Si nanosheets have been found to be sensitive to compressive strain. For the same magnitude of applied strain, compressive strain produces a larger induced strain than that of the applied tensile strain. The (110) Si nanosheet is easier to be compressed along the ⟨110⟩ direction. The (100) Si nanosheet undergoes a direct-to-indirect band gap transition under sufficient symmetrical strain and preserves a direct band gap characteristic up to a 10% asymmetrical strain. Under asymmetrical strain along ⟨100⟩, the direct band gap of the (110) Si nanosheet shows a linear relationship with the strain, which is a unique property advantageously exploitable in luminescence applications and opto-electronic devices. The (110) Si nanosheet

shows similar behavior when it is subjected to symmetrical and asymmetrical strain along ⟨110⟩. The variation in the strain dependence of Si nanosheets has been understood from an analysis of its decomposed charge density. The band structures of Si nanosheets can be manipulated to have different band gap characteristics by the application of different kinds of axial strains. Our findings highlight the immense potential of 2D Si nanostructures for applications in opto-electronics, luminescence, and solar cells through strain engineering.

AUTHOR INFORMATION

Corresponding Author

*E-mail: aprqz@cityu.edu.hk.

Present Addresses

†Beijing Computational Science Research Center, Beijing 100084, China.

ACKNOWLEDGMENT

The work described in this article is supported by a grant from the City University of Hong Kong [Project No. 7008092]; by the Centre for Functional Photonics (CFP) and Centre for Applied Computing and Interactive Media (ACIM) of City University of Hong Kong; and by the High Performance Cluster Computing Centre, Hong Kong Baptist University, which receives funding from Research Grant Council, University Grant Committee of the HKSAR and Hong Kong Baptist University. We thank Dr. C. S. Guo for helpful discussion.

REFERENCES

(1) Wolkin, M. V.; Jorne, J.; Fauchet, P. M.; Allan, G.; Delerue, C. *Phys. Rev. Lett.* **1999**, *82*, 197–200.
(2) Cui, Y.; Wei, Q.; Park, H.; Lieber, C. M. *Science* **2001**, *293*, 1289–1292.
(3) Ma, D. D. D.; Lee, C. S.; Au, F. C. K.; Tong, S. Y.; Lee, S. T. *Science* **2003**, *299*, 1874–1877.
(4) Nakano, H.; Mitsuoka, T.; Harada, M.; Horibuchi, K.; Nozaki, H.; Takahashi, N.; Nonaka, T.; Seno, Y.; Nakamura, H. *Angew. Chem., Int. Ed.* **2006**, *45*, 6303–6306.
(5) Kim, U.; Kim, I.; Park, Y.; Lee, K.-Y.; Yim, S.-Y.; Park, J.-G.; Ahn, H.-G.; Park, S.-H.; Choi, H.-J. *ACS Nano* **2011**, *5*, 2176–2181.
(6) Novoselov, K. S.; Geim, A. K.; Morozov, S. V.; Jiang, D.; Zhang, Y.; Dubonos, S. V.; Grigorieva, I. V.; Firsov, A. A. *Science* **2004**, *306*, 666–669.
(7) Okamoto, H.; Kumai, Y.; Sugiyama, Y.; Mitsuoka, T.; Nakanishi, K.; Ohta, T.; Nozaki, H.; Yamaguchi, S.; Shirai, S.; Nakano, H. *J. Am. Chem. Soc.* **2010**, *132*, 2710–2718.
(8) Sugiyama, Y.; Okamoto, H.; Mitsuoka, T.; Morikawa, T.; Nakanishi, K.; Ohta, T.; Nakano, H. *J. Am. Chem. Soc.* **2010**, *132*, 5946–5947.
(9) Kara, A.; Léandri, C.; Dávila, M.; De Padova, P.; Ealet, B.; Oughaddou, H.; Aufray, B.; Le Lay, G. *J. Supercond. Novel Magn.* **2009**, *22*, 259–263.
(10) Le Lay, G.; Aufray, B.; Léandri, C.; Oughaddou, H.; Biberian, J. P.; De Padova, P.; Dávila, M. E.; Ealet, B.; Kara, A. *Appl. Surf. Sci.* **2009**, *256*, 524–529.
(11) Aufray, B.; Kara, A.; Vizzini, S.; Oughaddou, H.; Leandri, C.; Ealet, B.; Le Lay, G. *Appl. Phys. Lett.* **2010**, *96*, 183102.
(12) Zhang, R. Q.; Lifshitz, Y.; Ma, D. D. D.; Zhao, Y. L.; Frauenheim, T.; Lee, S. T.; Tong, S. Y. *J. Chem. Phys.* **2005**, *123*, 144703.
(13) Guo, C. S.; Luo, L. B.; Yuan, G. D.; Yang, X. B.; Zhang, R. Q.; Zhang, W. J.; Lee, S. T. *Angew. Chem., Int. Ed.* **2009**, *48*, 9896–9900.
(14) Yang, X. B.; Zhang, R. Q. *Appl. Phys. Lett.* **2008**, *93*, 173108.
(15) Yang, X. B.; Guo, C. S.; Zhang, R. Q. *Appl. Phys. Lett.* **2009**, *95*, 193105.
(16) Lu, A. J.; Yang, X. B.; Zhang, R. Q. *Solid State Commun.* **2009**, *149*, 153–155.
(17) Haugerud, B. M.; Bosworth, L. A.; Belford, R. E. *J. Appl. Phys.* **2003**, *94*, 4102–4107.
(18) Lyons, D. M.; Ryan, K. M.; Morris, M. A.; Holmes, J. D. *Nano Lett.* **2002**, *2*, 811–816.
(19) Audoit, G.; Mhuircheartaigh, É. N.; Lipson, S. M.; Morris, M. A.; Blau, W. J.; Holmes, J. D. *J. Mater. Chem.* **2005**, *15*, 4809–4815.
(20) Morales, A. M.; Lieber, C. M. *Science* **1998**, *279*, 208–211.
(21) Goldthorpe, I. A.; Marshall, A. F.; McIntyre, P. C. *Nano Lett.* **2008**, *8*, 4081–4086.
(22) Goldthorpe, I. A.; Marshall, A. F.; McIntyre, P. C. *Nano Lett.* **2009**, *9*, 3715–3719.
(23) Peng, X.; Logan, P. *Appl. Phys. Lett.* **2010**, *96*, 143119.
(24) Perdew, J. P.; Burke, K.; Ernzerhof, M. *Phys. Rev. Lett.* **1996**, *77*, 3865–3868.
(25) Kresse, G.; Joubert, D. *Phys. Rev. B* **1999**, *59*, 1758–1775.
(26) Kresse, G.; Hafner, J. *Phys. Rev. B* **1994**, *49*, 14251–14269.
(27) Kresse, G.; Furthmüler, J. *Comput. Mater. Sci.* **1996**, *6*, 15–50.
(28) Monkhorst, H. J.; Pack, J. D. *Phys. Rev. B* **1976**, *13*, 5188–5192.
(29) Lu, A. J.; Zhang, R. Q.; Lee, S. T. *Appl. Phys. Lett.* **2007**, *91*, 263107.
(30) Hong, K.-H.; Kim, J.; Lee, S.-H.; Shin, J. K. *Nano Lett.* **2008**, *8*, 1335–1340.
(31) Huang, L.; Lu, N.; Yan, J.-A.; Chou, M. Y.; Wang, C.-Z.; Ho, K.-M. *J. Phys. Chem. C* **2008**, *112*, 15680–15683.
(32) Leu, P. W.; Svizhenko, A.; Cho, K. *Phys. Rev. B* **2008**, *77*, 235305.
(33) Logan, P.; Peng, X. *Phys. Rev. B* **2009**, *80*, 115322.
(34) Peng, X.; Alizadeh, A.; Kumar, S. K.; Nayak, S. K. *Int. J. Appl. Mech. Eng.* **2009**, *1*, 483–499.
(35) Gui, G.; Li, J.; Zhong, J. *Phys. Rev. B* **2008**, *78*, 075435.
(36) Williamson, A. J.; Grossman, J. C.; Hood, R. Q.; Puzder, A.; Galli, G. *Phys. Rev. Lett.* **2002**, *89*, 196803.
(37) Zhao, X.; Wei, C. M.; Yang, L.; Chou, M. Y. *Phys. Rev. Lett.* **2004**, *92*, 236805.
(38) Lu, A. J.; Zhang, R. Q. *Solid State Commun.* **2008**, *145*, 275–278.